

Impact of the regularization parameter in the Mean Free Path reconstruction method

M.A. Sánchez-Martínez,¹ F. Alzina,¹ J. Oyarzo,³ C.M. Sotomayor-Torres,^{1,3} and E. Chavez-Angel^{*1}

¹⁾ Catalan Institute of Nanoscience and Nanotechnology (ICN2), CSIC and The Barcelona Institute of Science and Technology (BIST), Campus UAB, Bellaterra, 08193 Barcelona, Spain.

²⁾ Instituto de Química, Pontificia Universidad Católica de Valparaíso, Casilla 4059, Valparaíso, Chile.

³⁾ ICREA- Institució Catalana de Recerca i Estudis Avançats, 08010 Barcelona, Spain.

*Corresponding author: emigdio.chavez@icn2.cat

The understanding of the mean free path (MFP) distribution of the energy carriers in materials (e.g. electrons, phonons, magnons, etc.) is a key physical insight into their transport properties. In this context, MFP spectroscopy has become an important tool to describe the contribution of carriers with different MFP to the total transport phenomenon. In this work, we revise the MFP reconstruction technique and present a study on the impact of the regularization parameter on the MFP distribution of the energy carriers. Furthermore, we introduce a new method to obtain the optimal value of this parameter using the L-curve criterion. This approach is applied to various transport phenomena at the nanoscale involving carriers of different physical nature and behaviour. These results demonstrated that the choice of the regularization parameter has a large impact on the physical information obtained from the reconstructed accumulation function, and thus cannot be chosen arbitrarily.

Keywords: Mean free path reconstruction, Mean free path distribution, ill-posed problem, Regularization Parameter, Tikhonov method.

Nomenclature		
Latin symbols		Greek symbols
A	Matrix that contain the integral kernel and the weight of the numerical integration.	α Transport property
CDF	Cumulative distribution function	β Weight of a given point for the quadrature of the numerical integration
d	Characteristic length of the sample	Λ Mean free path [m]
F_{acc}	Accumulation function	σ Interval of integration
FS	Fuchs-Sondheimer	μ Regularization parameter
GCV	Generalized cross validation	ξ Spin-Hall torque coefficient
K	Integral kernel	χ Knudsen number (Λ/d)
L	Period of the thermal transient gradient	
LSSE	Longitudinal spin Seebeck effect	
MFP	Mean free path	
n	Number of measurements	
m	Number of discretization points	
S	Suppression function	
SDL	Spin diffusion length	
T	Temperature [K]	
y	Variable of integration	
Subscripts		
	bulk	Property of the bulk
	c	cut off limit for MFP integration
	i	Normalised i -th measurement
	nano	Property of the nanostructure

I Introduction

In solid-state materials there is a variety of scattering mechanisms for energy carriers involved in different transport phenomena, such as impurities, boundaries, and collisions with other particles/quasi-particles. The average distance that a moving particle (photon, electron, etc.) or quasi particle (phonon, magnon, etc.) travels before being absorbed, attenuated, or scattered is defined as the mean free path (MFP). It is well known that energy carriers that propagate over different distances in a material having different MFP contribute differently to the energy transport. Thus the use of a single-averaged MFP may be inaccurate to describe the system[1,2].

It is possible to quantitatively describe how energy carriers with a specific MFP contribute to the total transport property by an MFP spectral function or MFP distribution[3], which contains the information of the specific transport property associated with the energy carriers with a certain MFP. By normalizing and integrating this spectral function we obtain the accumulation function, which describes the contribution of carriers with different MFPs below a certain MFP cut off to the total transport property, being very intuitive to identify which MFPs are the most relevant to the transport phenomenon under study by plotting this function.

When studying transport at the nanoscale, boundary scattering becomes important as the characteristic size of the nanostructure approaches the MFP of the carriers involved. From the bulk MFP distribution it is possible to predict how size reduction will affect a transport property in this material given that we know which MFPs are contributing the most. Inversely, it is possible to obtain the bulk MFP distribution from size-dependent experiments, where the critical size of each measurement acts as a MFP cut off due to boundary scattering.

This relation between the transport property at the nanoscale and the bulk MFP distribution is given by an integral transform. A suppression function, which accounts for the specific geometry of the experiment and depends upon the characteristic size of the structures and the MFP of the carriers, connects the bulk MFP distribution and the experimental measurements; acting in the kernel of the integral transformation. Using this integral relation it is possible to recover the MFP distribution from experimental data. This is known as the MFP reconstruction method[4].

This mathematical procedure however is an ill-posed problem with, in principle, infinite solutions. To obtain a physically meaningful result from it, some restrictions must be imposed. These constraints are mainly related to the shape of the mean free path distribution. The distribution is a cumulative distribution function (CDF) and it is subjected to some restrictions, e.g., the MFP distribution is unlikely to have abrupt steps because it is spread over such a wide range of MFPs. The distribution must thus obey some type of smoothness restriction[4]. Now, the problem becomes a minimization problem, where the solution lies in the best balance between the smoothness of the reconstructed function (solution norm) and its proximity to the experimental data (residual norm). This balance is controlled by the choice of the regularization parameter. The role of this parameter has been widely overlooked in the literature, where the choice of its value has been poorly justified and, in some occasions, it remains unmentioned. In this work we present a study of the impact that the choice of its value has in the reconstructed accumulation. We present a method to obtain the optimal value of this parameter using the L-curve criterion[5,6]. We apply it first to the thermal conductivity and the phonon-MFP distribution, and later we extended to magnon-mediated transport phenomena, namely, spin Seebeck effect and spin-Hall torque coefficient. We demonstrate that this methodology can be extended to several transport properties involving carriers of different physical nature and behaviour.

II Mean free path reconstruction method

To perform the reconstruction of the MFP distribution of the energy carriers, the only input needed is a characteristic suppression function and a well distributed set of experimental data, i.e., a large amount of experimental measurements spread over the different characteristic sizes of the system. The suppression function strongly depends on the specific geometry of the sample and the

experimental configuration. It relates the transport property of the nanostructure α_{nano} and that of the bulk α_{bulk} through the following expression:

$$\alpha_{\text{nano}} = S(\chi)\alpha_{\text{bulk}} \quad (1)$$

where χ is the Knudsen number $\chi = \Lambda_{\text{bulk}}/d$, Λ_{bulk} is the bulk MFP and d the characteristic length of the sample. The suppression function has been derived for different experimental geometries from the Boltzmann transport equation[7–9].

The relation between the transport coefficient $\alpha_{\text{nano}}(d)$ and the suppression function was originally derived for the thermal conductivity[4,10], and more recently has been proven to be applicable to the MFP of magnons and the spin diffusion length[11]. This relation can be expressed by means of a cumulative MFP distribution as

$$\alpha = \frac{\alpha_{\text{nano}}(d)}{\alpha_{\text{bulk}}} = - \int_0^\infty F_{\text{acc}}(\Lambda_{\text{bulk}}) \frac{dS(\chi)}{d\chi} \frac{d\chi}{d\Lambda_{\text{bulk}}} d\Lambda_{\text{bulk}} \quad (2)$$

where F_{acc} is the accumulation function,

$$F_{\text{acc}} = \frac{1}{\alpha_{\text{bulk}}} \int_0^{\Lambda_c} \alpha_{\Lambda}(\Lambda_{\text{bulk}}) d\Lambda_{\text{bulk}} \quad (3)$$

where α_{Λ} is the contribution to the total transport property of carriers with a mean free path Λ . This function represents the contribution of carriers with MFPs up to an upper limit, Λ_c , to the total transport property, and is the object that will be recovered by applying the MFP reconstruction technique.

From this definition it is easy to see that the accumulated function is subject to some physical restrictions: it cannot take values lower than zero for $\Lambda_c = 0$ or higher than one for $\Lambda_c \rightarrow \infty$, and it must be monotonous[4]. We can recognize that Eq. (2) is a Fredholm integral equation of the first kind that transforms the accumulation function $F_{\text{acc}}(\Lambda_{\text{bulk}})$ into a with $K = \frac{dS(\chi)}{d\chi} \frac{d\chi}{d\Lambda_{\text{bulk}}}$ acting as a kernel. Since the inverse problem of reconstructing the accumulation function F_{acc} is an ill-posed problem with infinite solutions[10]. Minnich[4] demonstrated that it can be discretised and the restrictions mentioned above can be imposed on F_{acc} to obtain a unique solution. Furthermore, it is reasonable to require the smoothness conditions mentioned before on F_{acc} , since it is unlikely to have abrupt behaviour in all its domain. These requirements can be applied through the Tikhonov regularization method, where the criterion to obtain the best solution F_{acc} is to find the following minimum:

$$\min\{\|A \cdot F_{\text{acc}} - \alpha_i\|_2^2 + \mu^2 \|\Delta^2 F_{\text{acc}}\|_2^2\} \quad (4)$$

where α_i is the normalised i -th measurement, $A = K(\chi_{i,j}) \times \beta_{i,j}$ is an $m \times n$ matrix, where m is the number of measurements and n the number of discretization points, $K_{i,j}$ is the value of the kernel at $\chi_{i,j} = \Lambda_{i,j}/d_i$, and $\beta_{i,j}$ the weight of this point for the quadrature. The operators $\|\cdot\|_2$ and Δ^2 are the

2-norm and the $(n-2) \times n$ trigonal Toeplitz matrix which represent a 2-nd order derivative operator, respectively. μ is the regularization parameter. The first term of Eq. 4 is related to how well our result fits to experimental data (residual norm), while the second term represents the smoothness of the accumulation function (solution norm). The balance between both is controlled by the regularization parameter μ . In other words μ sets the equilibrium between how good the experimental data is fitted and how smooth is the fitting function. The choice of μ will thus have a huge impact on the final result of the accumulation function, and a criterion to obtain the optimal value must be established. This is still an open question in mathematics. Several heuristic methods are frequently used, such as the Morozov's discrepancy principle, the Quasi-Optimally criterion or the generalized cross validation (GCV)[5,6].

In our study we will use the L-curve criterion[5,6], which establishes that the optimal balance between the residual norm and the solution norm is found by locating a distinct point in the three-dimensional curve obtained by plotting the residual norm vs the solution norm, parametrized by the regularization parameter. It has been found that the corresponding point lies in the corner of the L-curve in the residual norm-solution norm plane, which can be defined as the point of maximum curvature. The optimal value of μ can be found by locating the peak position of the curvature as a function of μ [5,6].

The method employed is depicted in Fig. 1, and is common to all cases presented here. The experimental data in the case studies shown in this work was reproduced from the digitalization of the images and the corresponding uncertainties. A specific suppression function is selected for each case, depending on the particular geometry and experimental configuration. As explained above, the integral in Eq (2) is discretized, and an adequate integration interval depending on the span of experimental data is chosen. At this point, instead of introducing an arbitrary value of the regularization parameter, we determine the optimal value via the L-curve criterion. We have observed that the distribution of the curvature depending on $\log \mu$ follows a Gaussian distribution, thus allowing us to obtain the peak, i.e., the highest curvature (corresponding to the corner of the L-curve), using a Gaussian fitting with a reduced number of computational points. With this optimal value of the regularization parameter we can proceed to apply the Tikhonov regularization method and impose the conditions on F_{acc} using a convex optimization package for MATLAB called CVX[12,13], thus obtaining an accurate accumulation function.

III. Case studies

The MFP reconstruction method, as well as the method here presented for the selection of μ , does not require a priori any physical assumption about the carrier, such as band structure or velocity. In this section, we apply the method to various carriers and transport phenomena of different physical nature to demonstrate its wider validity.

A. Phonons in out-of-plane thermal transport in graphite

Firstly, we will study the MFP reconstruction of phonons in cross-plane thermal transport along the c-axis of graphite. The experimental thermal conductivities were obtained from a set of graphite samples with different thickness and measured at different temperatures by Zhang et al.[14]¹³. From this experimental data, we will recover the MFP distribution in bulk graphite by using the L-curve criterion based MFP reconstruction method. This will illustrate the different steps and details which apply to all of the cases that we present here.

As shown in Fig. 1 after obtaining the experimental data the only input needed is the suppression function. In this case, we will employ the Fuchs-Sondheimer cross-plane suppression function, described by[15]

$$S(\chi) = 1 - 3\chi \left(\frac{1}{4} - \int_0^1 y^3 e^{-1/(xy)} dy \right) \quad (5)$$

The dependence of both the reduced norm and the solution norm on μ can be visualized as a 3-D curve (see Fig. 2), and the projection of this curve on the solution norm-reduced norm plane is the L-curve, named after its characteristic shape.

Fig. 3 shows the curvature distribution of $\|A \cdot F_{acc} - \alpha_i\|_2$ vs $\|\Delta^2 F_{acc}\|_2$ as a function of $\log \mu$ at temperature $T = 40$ K. This behaviour is similar at all the temperatures considered, ranging from 40 K to 294 K. In order to see the influence of the suppression function in the optimal value of μ , we calculated the optimal value for an exponential suppression function, $S = 1 - e^{-1/\chi}$, as a representative example of one of the simplest descriptions of transport. In Fig. 4 we show the optimal value of μs obtained using the cross-plane FS and the exponential-like suppression functions for different temperatures in the case under study.

The reconstructed accumulation function is shown in Fig. 5(a). We can see that for the optimal value of, the MFP of the carriers spans $100 \text{ nm} < \Lambda < 2000 \text{ nm}$. One common accepted criterion is using as a regularization parameter the first value of that returns a smooth accumulation function[9]. In this case, we can see that the election of $\mu = 0.1$ yields a completely different accumulation function. With $\mu = 0.1$ the span of the MFP distribution has been shrunk one order of magnitude, from 300 nm to 600 nm. If we set $\mu = 4$, the reconstructed accumulation function will be very smooth, and the MFP of the carriers spans from a few nanometres up to several thousand though it fits the data poorly.

The choice of μ does not only impact in the accumulation function. The influence of μ on the solution norm can be seen in Fig. 5(b). By choosing a very low value for μ , the weight of the optimization method lies on the reduced norm $\|A \cdot F_{acc} - \alpha_i\|_2$, thus yielding a narrower, spikier accumulation function and a better correspondence of the recovered thermal conductivity with those obtained experimentally. On the contrary, when choosing a high value for μ , the optimization method focuses on the smoothness of the function, producing an accumulation function with zero 2nd order derivative and a poor correspondence with the experimental data.

B. In-plane thermal transport in Si membranes

The second case study is the in-plane thermal transport in a 400 nm Si membrane at room temperature obtained using the Thermal Transient Grating (TTG) technique, obtained from Johnson et al.[16]. In the previous example the characteristic length of the system was the thickness of the graphite sheets. Here the Si membrane has fixed thickness d and the variable length scale is the period of the thermal grating L . Since the measurement of in-plane thermal conductivity in the membrane will correspond to phonons with MFPs lower than L in each measurement, the grating period becomes the equivalent of the maximum MFP.

For this case we will use a combination of two suppression functions[8]. The suppression function derived for this particular measurement geometry is given by[16]

$$S_1(q\Lambda) = \frac{3}{q^2 \Lambda^2} \left(1 - \frac{\arctan(q\Lambda)}{q\Lambda} \right) \quad (6)$$

where $q = 2\pi/L$ is the grating wavevector.

This function is unity in the limit $q\Lambda \ll 1$, in the diffusive limit, and goes like $(q\Lambda)^{-2}$ for $q\Lambda \gg 1$, in the ballistic regime, thus describing the transition between both regimes necessary to adequately interpret the measured quantities in the experiment[16]. It is also necessary to account for the boundary scattering in the membrane, which is described by the Fuchs-Sondheimer suppression function for in-plane thermal transport[10]

$$S_2(\chi) = 1 - \frac{3}{8}\chi + \frac{3}{2}\chi \int_1^\infty (y^{-3} - y^{-5})e^{-y/\chi} dy \quad (7)$$

where χ is the Knudsen number $\chi = \Lambda_{\text{bulk}}/d$.

Similarly to the previous case, we obtain the optimal value of μ using a Gaussian fit to obtain a value $\mu_{\text{opt}} = 1.052$ at room temperature. In Fig. 6 we can see the effect of the different values of μ . Note that, in this case, the reduction of μ affects mainly the smoothness of the reconstructed function, reflecting the observed changes on the concavity and convexity of the accumulation function on to the behaviour of the solution norm with the variations in μ . The increase of the regularization parameter beyond the optimal value results in an increase of the span of the MFP of the carriers, as shown in Fig. 6(a), and a poor agreement with the experimental data, as can be seen in Fig. 6(b).

It should be noted that, since the range of data is finite, we must set an adequate range of computational points to integrate of the suppression function.

In Fig. 7, for a small integration interval σ (red line) the reconstructed accumulation function is smooth and the span of MFP is reasonable, but is important to pay attention to the graph in the inset showing the recovered thermal conductivity corresponding to the different accumulation functions. In this case the thermal conductivity starts to decrease with increasing transient grating period (increasing MFP), which is unreasonable. Increasing σ (green line), we see that the accumulation function is smooth with an adequate span of MFP, and the corresponding thermal conductivity becomes monotonic. If we keep increasing this integration interval (blue line) the thermal conductivity remains monotonic, but the accumulation function becomes unphysical, since by adding more carriers with higher MFP, the accumulation function decreases.

This is a source of error unrelated to the regularization parameter and is an important consideration when setting the parameters for the MFP reconstruction code in order to obtain physically relevant results.

C. In-Plane Thermal transport in Si: Reconstruction by changing the thickness of the membrane.

The dependence of the reconstructed accumulation function on the regularization parameter relies on the L-curve and the dependence of the residual norm $\|A \cdot F_{\text{acc}} - \alpha_t\|_2$ and solution norm $\|\Delta^2 F_{\text{acc}}\|_2$ on μ . The following case illustrates example of how the particular shapes of these different curves can strongly affect the reconstruction.

The data was obtained by Cuffe *et al.*[10] for Si membranes with thickness ranging from 15 to 1518 nm. As we can see in Fig. 8, the L-curve (blue) is similar to that presented for the cross-plane thermal transport in graphite in Fig. 2. The main differences with the cases studied here are the μ -dependence of the solution and residual norm, represented by the green and red curves, respectively, in Fig. 8. We can see that the μ -dependence of the solution norm (green line, Fig. 8) is different from that presented in Fig. 2, where the increase of the solution norm is uniform with the increasing of μ . This is reflected

in the impact of increasing μ . This is reflected in the impact of μ in the accumulation function and recovered thermal conductivity, as can be seen in Fig. 9.

On the one hand, it is easy to see that the variation of the solution norm from $\mu = 1$ to $\mu = 3$ is smaller than that from $\mu = 3$ to $\mu = 4$ and similar to the increment in the smallest range $\mu = 0.1$ to $\mu = 1$, in contrast with the uniform increase observed in Fig. 2. The immediate consequence of this is that, as we can see in Fig. 9(a), there are no major differences neither in the smoothness nor in the span of the accumulated reconstructed function when we move from $\mu_{\text{opt}} = 1.0924$ to $\mu = 3$, and the steps and jumps observed in the accumulation function for $\mu = 0.1$ correspond to the behaviour of the solution norm and its dependence on μ in this region, as mentioned before in Fig. 6. On the other hand, the red curve in Fig. 8 representing the dependence of the residual norm on μ becomes flat very quickly compared to that shown in Fig. 2. We can see in Fig. 9 that the recovered thermal conductivity corresponding to the different accumulation function does not change significantly when we choose $\mu = \mu_{\text{opt}}$ or $\mu = 3$.

The L-curve criterion is efficient to obtain the most adequate regularization parameter, but in this case the reconstructed accumulation function is very robust against changes in μ due to the particular flatness of the residual and solution norm depending on the values of μ .

It is worth noting the difference between the MFP distribution obtained for bulk Si in Fig. 9(a) and that obtained for the 400 nm thickness Si membrane in Fig. 6(a) for their respective optimal reconstruction parameters. This is a good example of the importance of the choice of the reconstruction parameter in order to obtain a physically-meaningful result.

D Magnon-mediated longitudinal spin-Seebeck effect in YIG films

This data was obtained by Guo *et al*[17] measuring the thickness dependence of the longitudinal-Spin Seebeck effect (LSSE) in YIG films. The suppression function used in the reconstruction was the Fuchs-Sondheimer model presented in Eq. (7). In Fig. 10(a) it is easy to see that the different values of μ have an impact mainly in the accumulation function, being the case of the lower value of μ that affects the most both the accumulation function and the recovered LSSE, as shown in Fig. 10(b).

The reconstructed function for the optimal value $\mu_{\text{opt}} = 0.8856$ at T=250K is shown in Fig. 10. The optimal value of the reconstruction parameter was calculated for all the temperatures measured, obtaining a different value for each of them (see Fig. 11).

E Spin diffusion length in Pt films

This case is an example of the application of this technique to a completely different transport phenomena, namely, the spin diffusion length. The experiment consisted of measuring the thickness dependence of the spin-Hall torque coefficient, ξ , in platinum[18] .

In this case, the suppression function is derived from the drift-diffusion model[19], and given by[20]

$$S(\chi) = 1 - \frac{1}{\sinh(1/\chi)} \quad (8)$$

This case differs from the previous phenomena, having a narrow span of the MFP distribution. For the optimal value of μ , the accumulation function's range goes from around 0.7 to 2 nm, and for $\mu = 0.1$ it shrinks to be from 1 to 2 nm (see Fig. 12). This indicates that the method is very sensitive even for very narrow MFP distributions, which allows it to be applied to a wide range of transport phenomena.

IV. CONCLUSIONS

We have demonstrated that the choice of the regularization parameter μ has a large impact on the physical information obtained from the reconstructed accumulation function, and thus cannot be chosen arbitrarily. We have also demonstrated that the same value of μ cannot be employed to reconstruct the accumulation function at different temperatures, and that choice of this value needed to be studied and justified. The result presented here indicate that a solid criterion to choose the value of the reconstruction parameter is needed, and that the reconstruction process must be performed individually for each temperature. We have established a robust method to reconstruct the accumulation function estimating the optimal value of the reconstruction parameter, using the L-curve criterion, to obtain the most adequate reconstruction.

The method presented here can be applied to many different cases. The only input needed to reconstruct the mean free path distribution of the carriers is a well-known suppression function and a well distributed set of experimental data points. Regardless of the carrier physical behaviour or the span of MFP, we have proven the method to be applicable, and we have seen that the robustness of the reconstruction against deviations from the estimated value of μ will depend on the particular variation of the solution norm and reduced norm with μ .

Acknowledgements

The authors acknowledge the financial support from the EU FP7 project QUANTIHEAT (Grant No 604668) and the Spanish MINECO-Feder project PHENTOM (FIS2015-70862-P). M.A.S-M. acknowledges support from SO-FPI fellowship BES 2015-075920. ICN2 acknowledges support from Severo Ochoa Program (MINECO, Grant SEV-2013-0925) and funding from the CERCA Programme/ Generalitat de Catalunya. We thank Dr. G. Whitworth for a critical reading of the manuscript.

References

- [1] N.W. Ashcroft and N.D. Mermin, *Solid State Physics*, Saunders College, 1976.
- [2] T.M. Tritt, ed., *Thermal Conductivity: Theory, Properties, and Applications*, Physics of Solids and Liquids Springer US, 2004.
- [3] F. Yang and C. Dames, "Mean free path spectra as a tool to understand thermal conductivity in bulk and nanostructures", *Phys. Rev. B*, vol. 87, no. 3, pp. 35437, 2013. DOI: 10.1103/PhysRevB.87.035437.
- [4] A.J. Minnich, "Determining phonon mean free paths from observations of quasiballistic thermal transport", *Phys. Rev. Lett.*, vol. 109, no. 20, pp. 205901, 2012. DOI: 10.1103/PhysRevLett.109.205901.
- [5] P.C. Hansen and D.P. O'Leary, "The use of the L-curve in the regularization of discrete ill-posed problems", *SIAM J. Sci. Comput.*, vol. 14, no. 6, pp. 1487–1503, 1993. DOI: 10.1137/0914086.
- [6] P.C. Hansen, *The L-curve and its use in the numerical treatment of inverse problems*, in *Computational Inverse Problems in Electrocardiology*, P. Johnston, ed., WIT press, 2000, pp. 119–142.
- [7] V. Chiloyan, L. Zeng, S. Huberman, A.A. Maznev, K.A. Nelson and G. Chen, "Variational approach to extracting the phonon mean free path distribution from the spectral Boltzmann transport equation", *Phys. Rev. B*, vol. 93, no. 15, pp. 155201, 2016. DOI: 10.1103/PhysRevB.93.155201.
- [8] C. Hua and A.J. Minnich, "Transport regimes in quasiballistic heat conduction", *Phys. Rev. B*,

vol. 89, no. 9, pp. 94302, 2014. DOI: 10.1103/PhysRevB.89.094302.

- [9] L. Zeng, K.C. Collins, Y. Hu, M.N. Luckyanova, A.A. Maznev, S. Huberman et al., "Measuring Phonon Mean Free Path Distributions by Probing Quasiballistic Phonon Transport in Grating Nanostructures", *Sci. Rep.*, vol. 5, no. 1, pp. 17131, 2015. DOI: 10.1038/srep17131.
- [10] J. Cuffe, J.K. Eliason, A.A. Maznev, K.C. Collins, J.A. Johnson, A. Shchepetov et al., "Reconstructing phonon mean-free-path contributions to thermal conductivity using nanoscale membranes", *Phys. Rev. B*, vol. 91, no. 24, pp. 245423, 2015. DOI: 10.1103/PhysRevB.91.245423.
- [11] E. Chavez-Angel, R.A. Zarate, S. Fuentes, E.J. Guo, M. Kläui and G. Jakob, "Reconstruction of an effective magnon mean free path distribution from spin Seebeck measurements in thin films", *New J. Phys.*, vol. 19, no. 1, pp. 13011, 2017. DOI: 10.1088/1367-2630/aa5163.
- [12] M. Grant and S. Boyd, *Graph implementations for nonsmooth convex programs*, in *Recent advances in learning and control*, V. Blondel, S. Boyd and H. Kimura, eds., Springer-Verlag Limited, 2008, pp. 95–110.
- [13] *CVX: Matlab software for disciplined convex programming, version 2.1*. Available at <http://cvxr.com/cvx>.
- [14] H. Zhang, X. Chen, Y.-D. Jho and A.J. Minnich, "Temperature-Dependent Mean Free Path Spectra of Thermal Phonons Along the c -Axis of Graphite", *Nano Lett.*, vol. 16, no. 3, pp. 1643–1649, 2016. DOI: 10.1021/acs.nanolett.5b04499.
- [15] C. Hua and A.J. Minnich, "Semi-analytical solution to the frequency-dependent Boltzmann transport equation for cross-plane heat conduction in thin films", *J. Appl. Phys.*, vol. 117, no. 17, pp. 175306, 2015. DOI: 10.1063/1.4919432.
- [16] J.A. Johnson, A.A. Maznev, J. Cuffe, J.K. Eliason, A.J. Minnich, T. Kehoe et al., "Direct Measurement of Room-Temperature Nondiffusive Thermal Transport Over Micron Distances in a Silicon Membrane", *Phys. Rev. Lett.*, vol. 110, no. 2, pp. 25901, 2013. DOI: 10.1103/PhysRevLett.110.025901.
- [17] E.-J. Guo, J. Cramer, A. Kehlberger, C.A. Ferguson, D.A. McLaren, G. Jakob et al., "Influence of thickness and interface on the low-temperature enhancement of the spin Seebeck effect in YIG films", *Phys. Rev. X*, vol. 6, no. 3, pp. 31012, 2016. DOI: 10.1103/PhysRevX.6.031012.
- [18] M.-H. Nguyen, D.C. Ralph and R.A. Buhrman, "Spin torque study of the spin Hall conductivity and spin diffusion length in platinum thin films with varying resistivity", *Phys. Rev. Lett.*, vol. 116, no. 12, pp. 126601, 2016. DOI: 10.1103/PhysRevLett.116.126601.
- [19] P.M. Haney, H.-W. Lee, K.-J. Lee, A. Manchon and M.D. Stiles, "Current induced torques and interfacial spin-orbit coupling: Semiclassical modeling", *Phys. Rev. B*, vol. 87, no. 17, pp. 174411, 2013. DOI: 10.1103/PhysRevB.87.174411.
- [20] A. Kehlberger, U. Ritzmann, D. Hinzke, E.-J. Guo, J. Cramer, G. Jakob et al., "Length scale of the spin Seebeck effect", *Phys. Rev. Lett.*, vol. 115, no. 9, pp. 96602, 2015. DOI: 10.1103/PhysRevLett.115.096602.

Figures

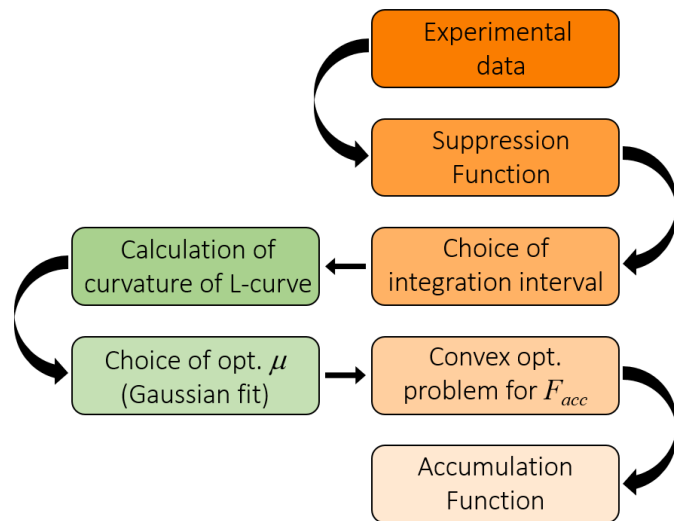


Figure 1 Flow-chart of the reconstruction method used to obtain the accumulation function from experimental data

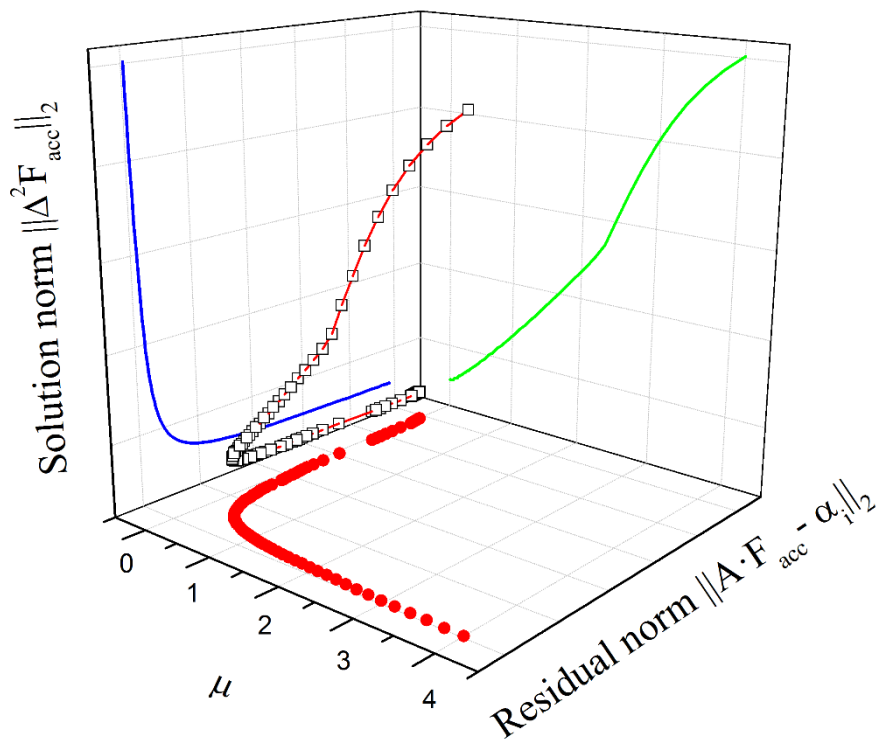


Figure 2 3-D visualization of the relation between the L-Curve (blue) and the different values of μ for a Fuchs-Sondheimer suppression function at $T=250$ K for graphite measurements.

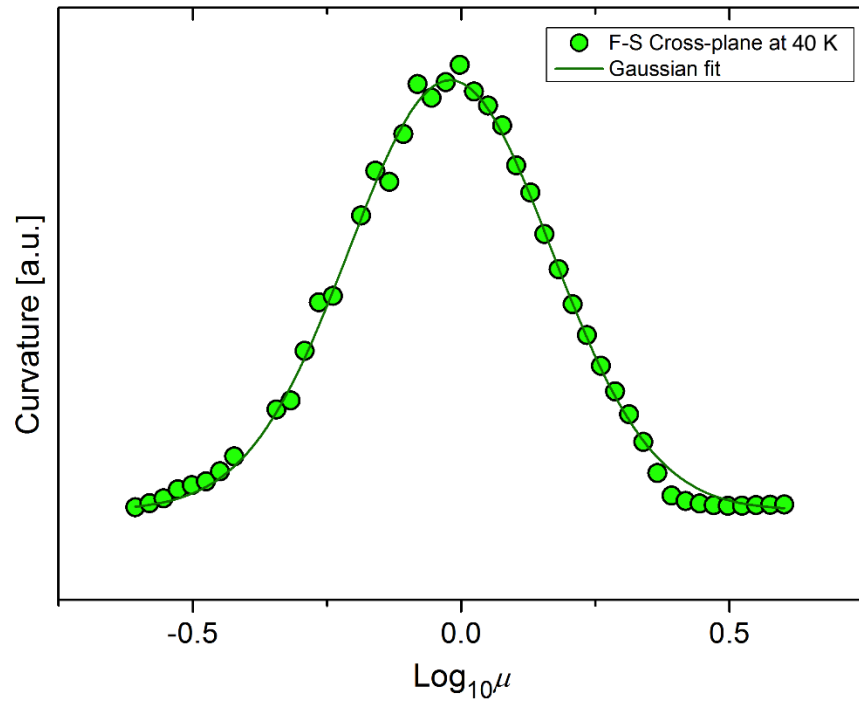


Figure 3 Curvature distribution over $\log \mu$ for the L-Curve corresponding to cross-plane thermal transport in graphite at $T = 40$ K using the FS suppression function.

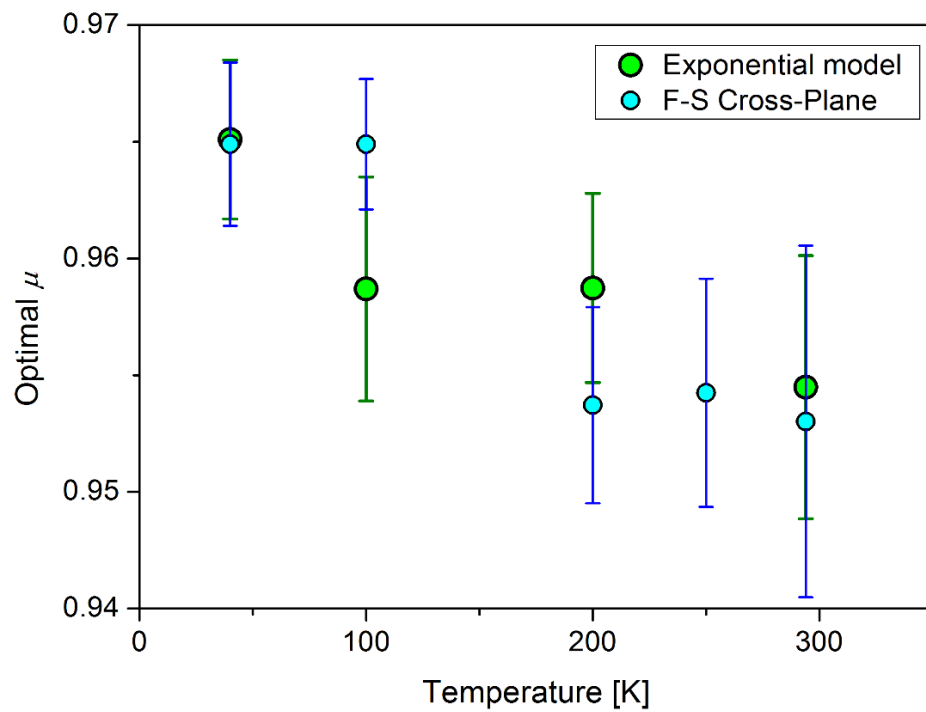


Figure 4 Optimal values of μ calculated as the peak of the Gaussian distribution for the different temperatures using the FS cross-plane and an exponential-like suppression functions for the graphite experiments.

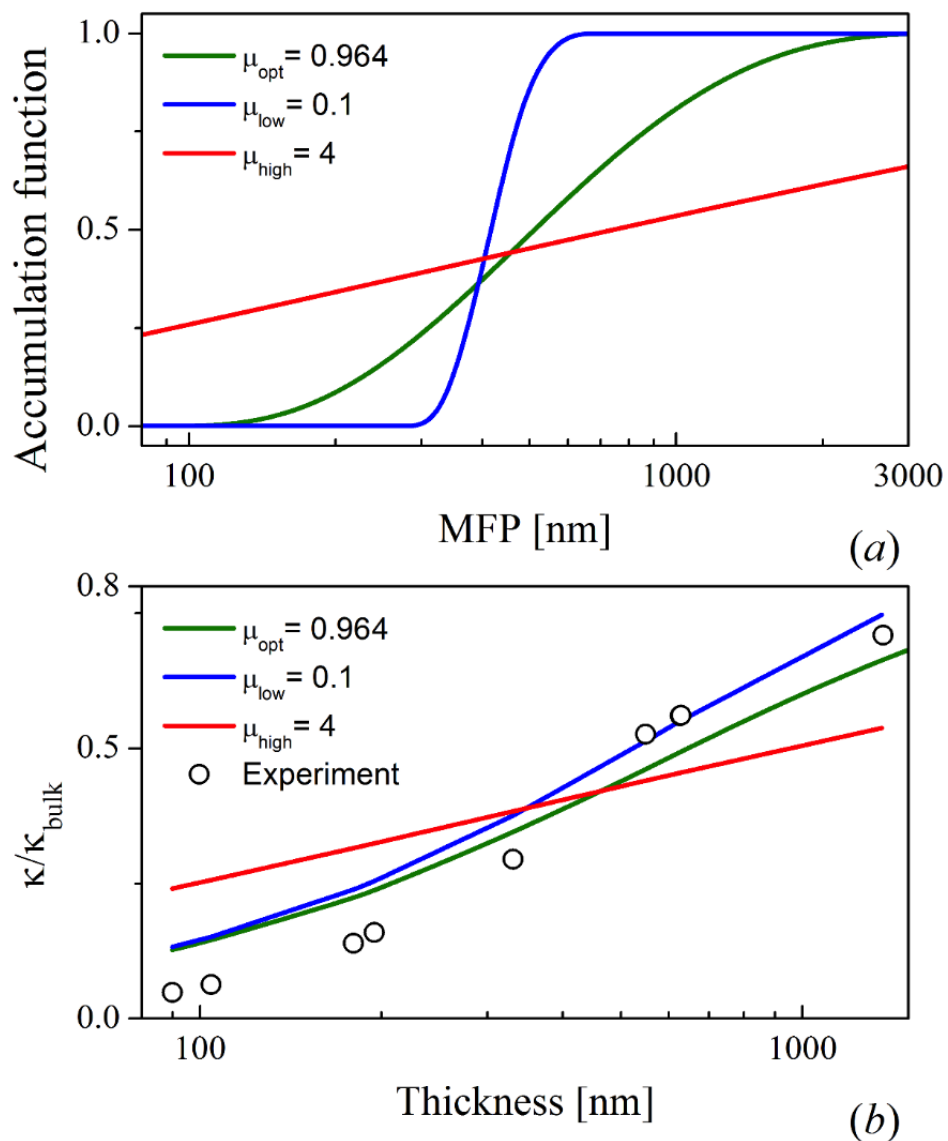


Figure 5 (a) Phonon mean free path distribution of the accumulation function reconstructed for μ_{opt} (green) using the FS cross-plane suppression function. The blue and red lines are the result obtained using a low and high value of μ , respectively. **(b)** Thermal conductivity normalized to the bulk value corresponding to the accumulation functions (red, green, and blue) for different thickness of the graphite sample[14].

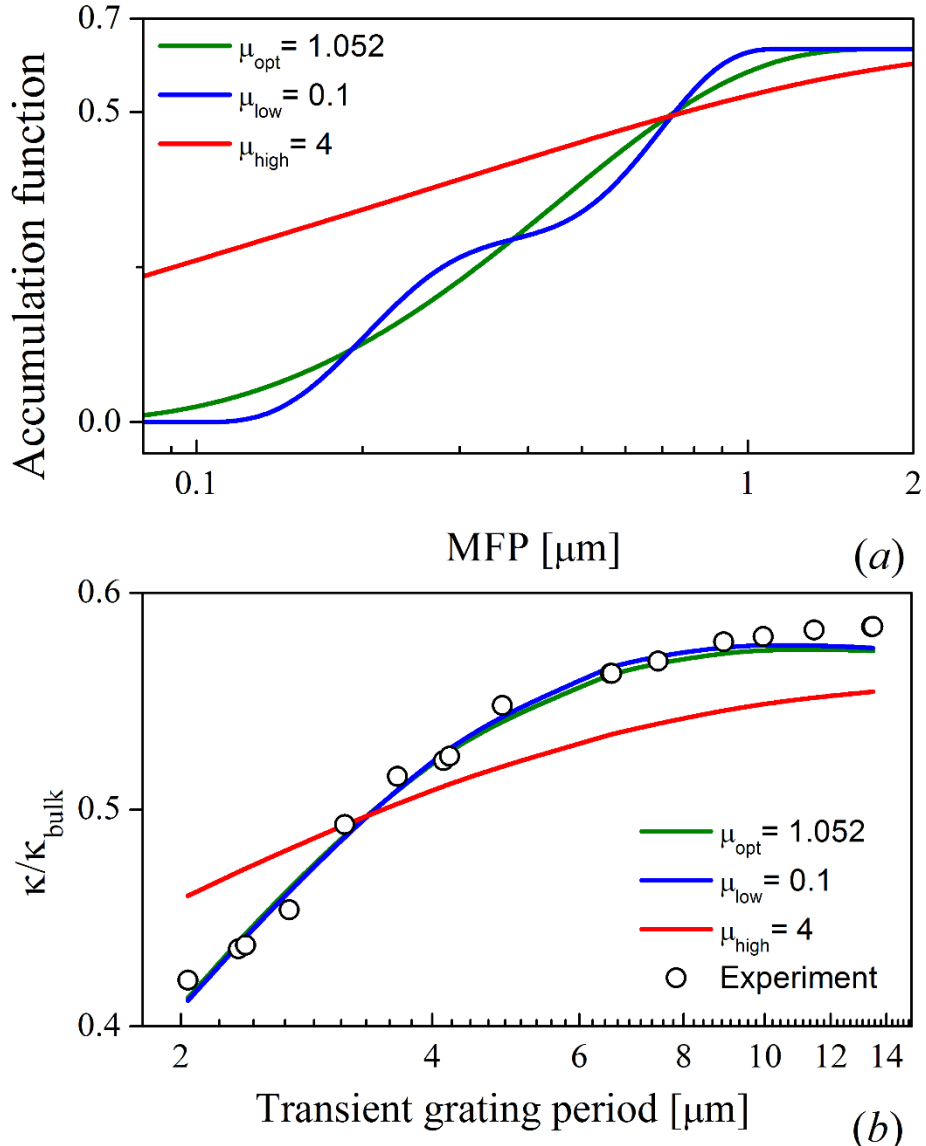


Figure 6 (a) Phonon mean free path distribution of the accumulation function for a 400 nm Si film reconstructed for μ_{opt} (green line). The blue and red lines are the result obtained using a low and high value of μ , respectively. **(b)** Thermal conductivity of 400 nm Si film corresponding to the different accumulation functions (red, green, and blue lines) for different transient grating periods in the experimental technique [16]

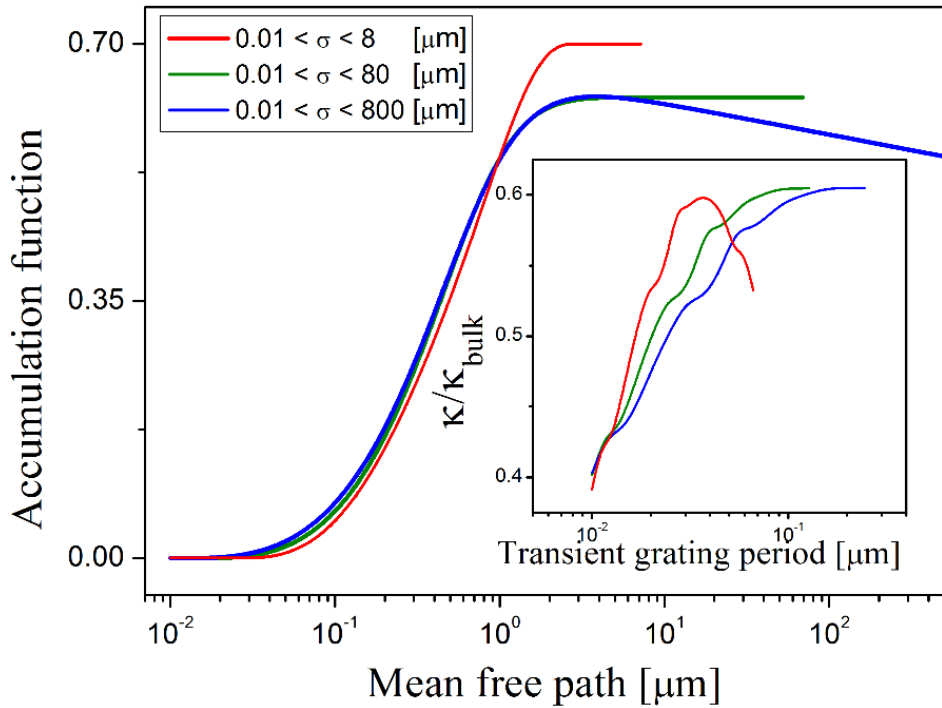


Figure 7 Impact of the integration interval on the accumulation function and in the recovered thermal conductivity (inset) for a small, adequate and large integration interval (red, green, and blue lines, respectively) of 400 nm Si film transient grating experiments.

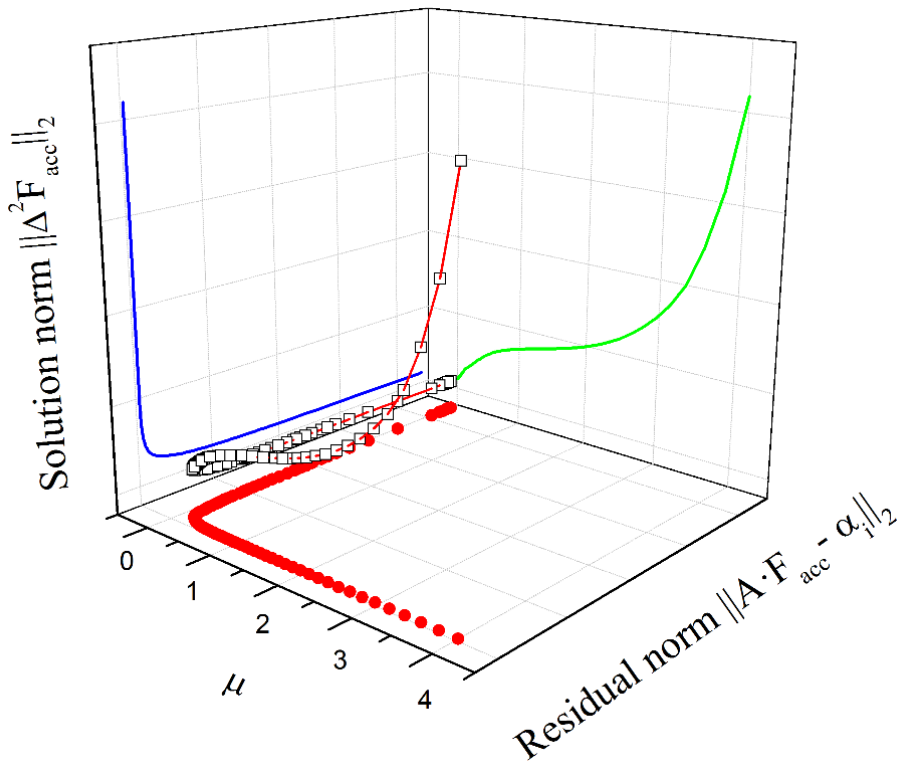


Figure 8 3-D visualization of the relation between the L-curve (blue line), the solution norm, the residual norm, and the different values of μ . The curve was obtained using 400 nm Si film transient grating experiments.

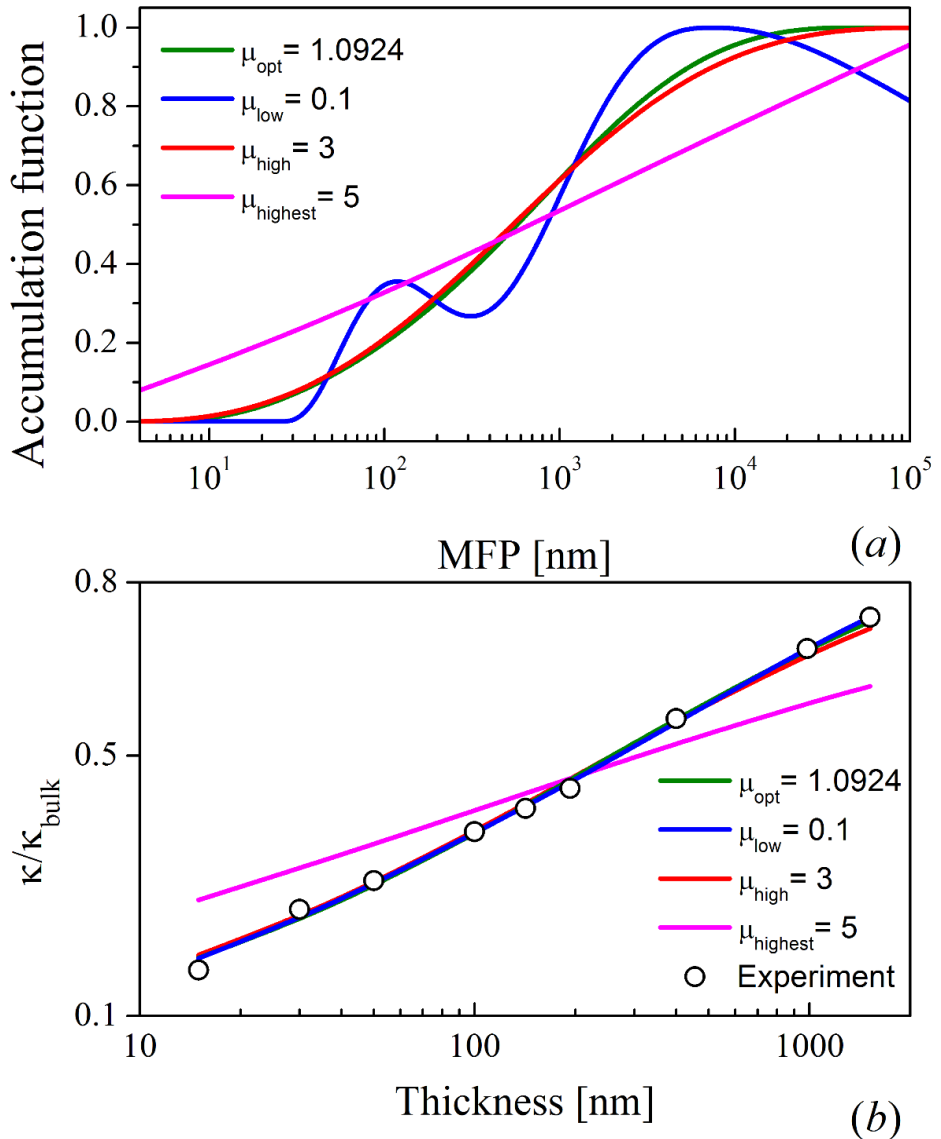


Figure 9 (a) Phonon mean free path distribution of bulk Silicon reconstructed from the thickness dependence of thermal conductivity. The green, blue, red and pink lines represent reconstructions for different values the μ : optimum μ_{opt} , a small μ_{low} , a high μ_{high} and a very large μ_{highest} values, respectively. **(b)** Thermal conductivity corresponding to the different accumulation functions (red, green, blue and pink lines) for different samples with different thickness[10].

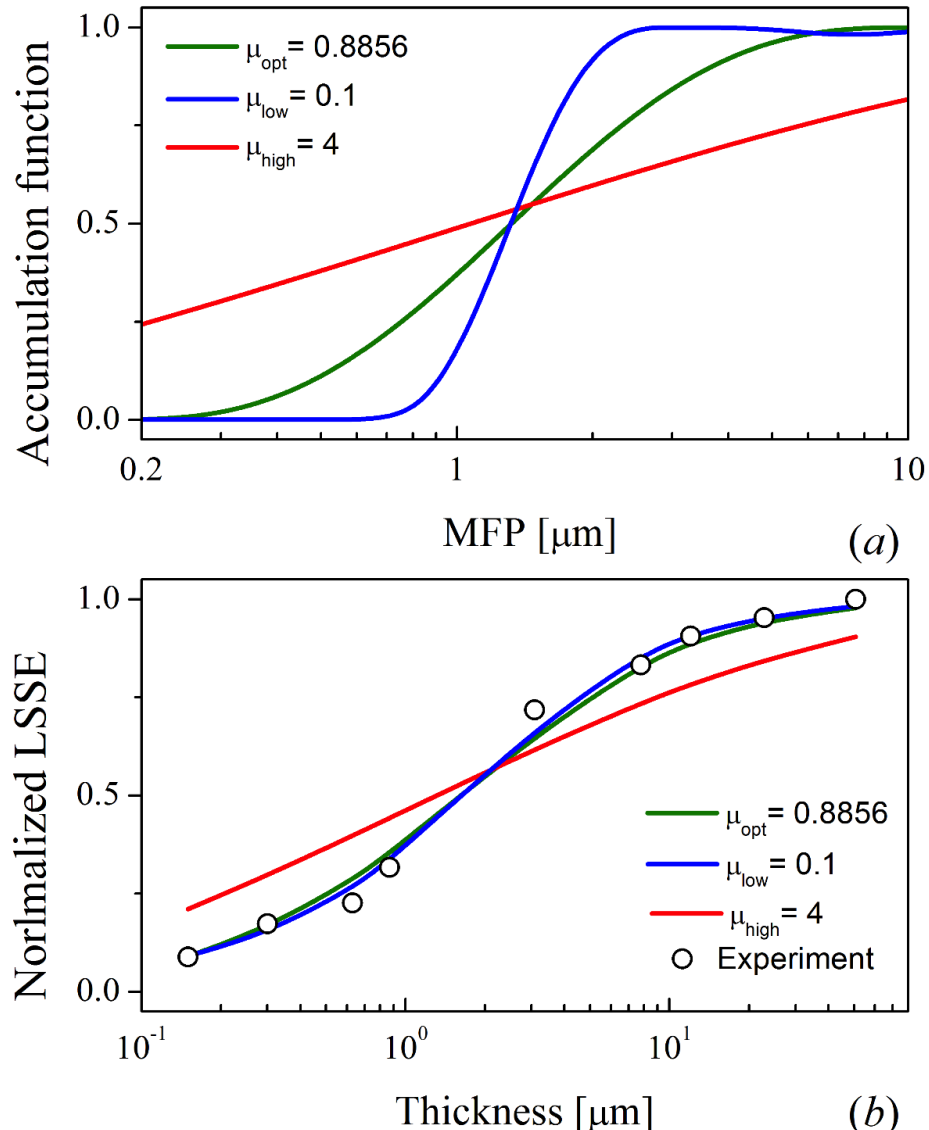


Figure 10 (a) Magnon mean free path distribution of the accumulation function reconstructed for μ_{opt} (green line) for spin Seebeck effect experiments. The blue and red lines are the result obtained using a low and high value of μ , respectively. **(b)** Normalized Longitudinal Spin-Seebeck coefficient for different thickness of the YIG sample [17].

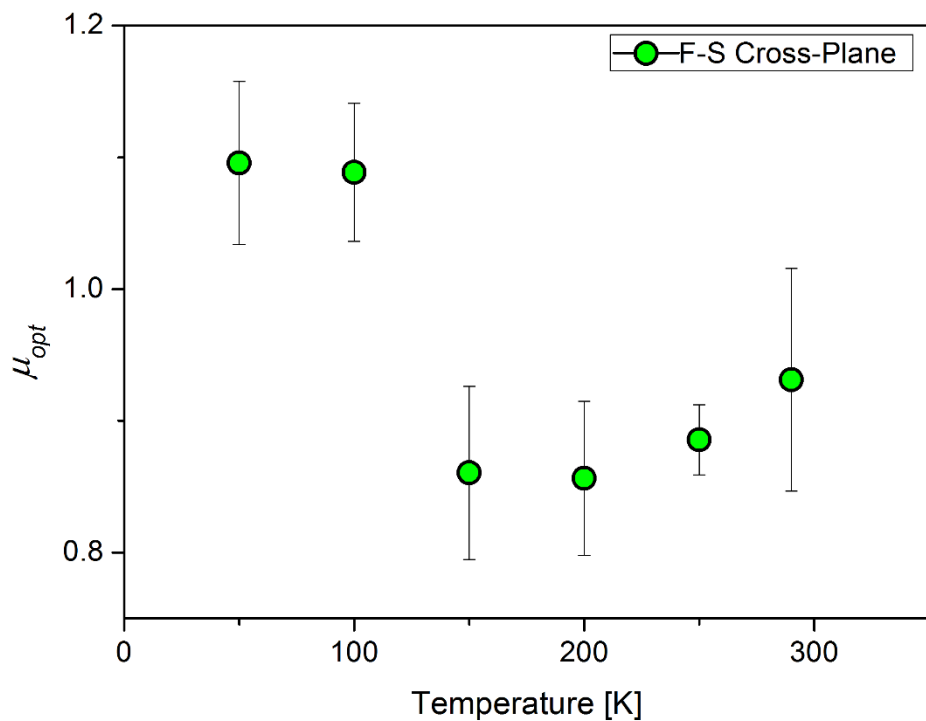


Figure 11 Optimal values of μ for the Magnon-MFP reconstruction at different temperatures for LSSE experiments.

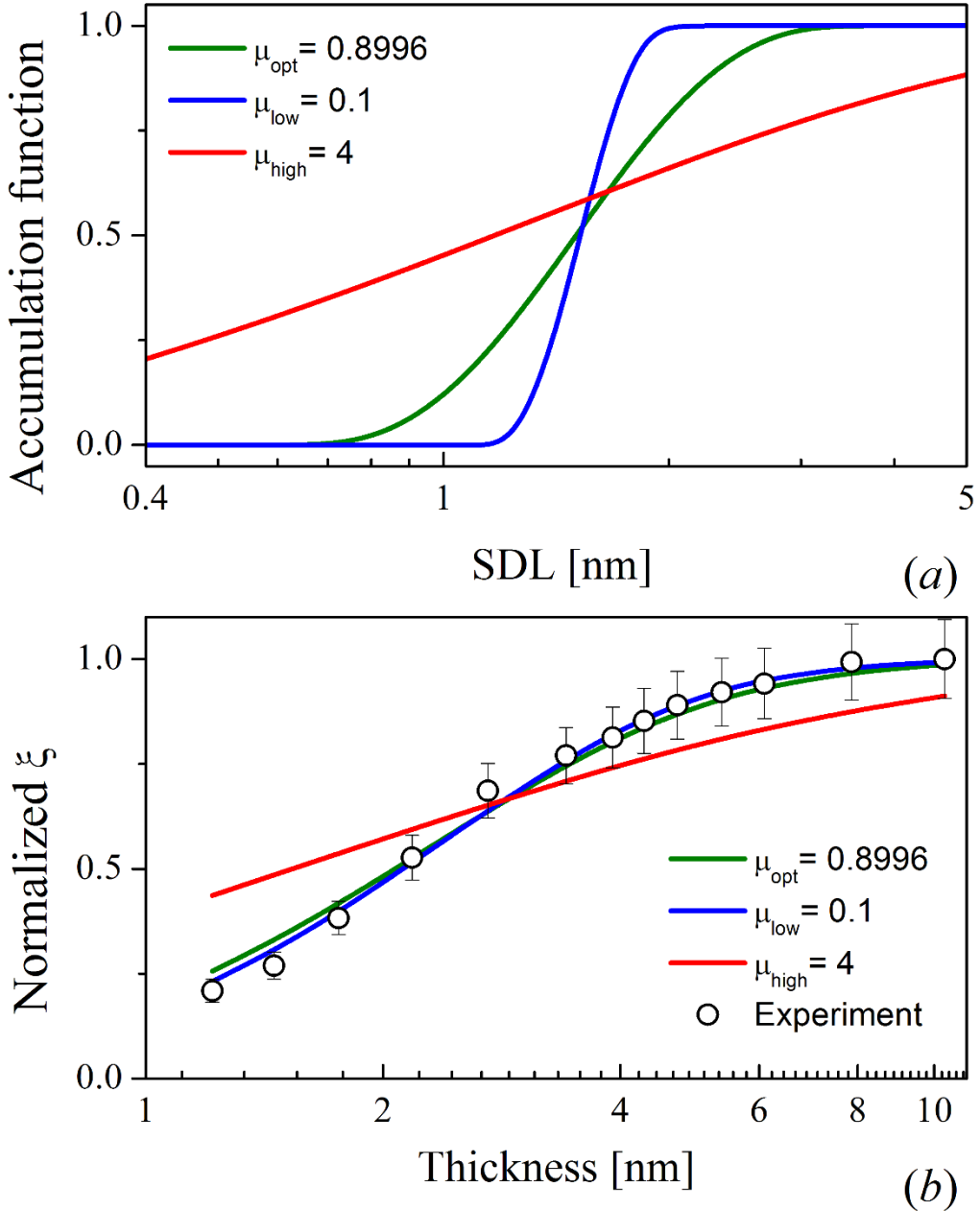


Figure 12 Spin diffusion length distribution of the accumulation function reconstructed for spin-Hall torque experiments. The blue and red lines are the result obtained using a low and high value of μ , respectively. The green line represent the MFP distribution reconstructed using μ_{opt} . (b) Normalized Longitudinal spin-Hall torque coefficient for different thickness of the Pt film [18].